Journal of Sound and Vibration (1998) **215**(1), 47–62
Article No. sv981576

DYNAMIC PROBLEMS CONCERNING THE SPEED OF ROTATION INCREASE OF A TURBINE–BLOWER ASSEMBLY

A. Castilho
PETROBRAS, *Avenida Republica do Chile* 65, 20035-900 *Rio de Janeiro-RJ*, *Brazil*

AND

G. Jacquet-Richardet and M. Lalanne
Institut National des Sciences Appliquées de Lyon, *Laboratoire de Mécanique des Structures*, *UPRESA*-5006-*CNRS*, 20 *Avenue Albert Einstein*, 69621 *Villeurbanne*, *France*

(*Received* 19 *November* 1997, *and in final form* 23 *February* 1998)

This paper investigates the dynamic problems of a turbine–blower assembly when its speed of rotation is increased by roughly ten per cent to obtain better efficiency. Changes concerning the dynamic behaviour of rotors in torsion and in bending, the dynamic behaviour of blades and the stresses in blades, have been estimated. It is shown that some modifications are necessary in order to allow the required increased speed.

1. INTRODUCTION

In 1973, during the start-up of a turbine–blower assembly, see Figure 1, of the RPBC (Refineria Presidente Bernardes—Cubatao), situated nearby Sao Paulo, tests showed natural torsional frequencies which could be excited in the operating range of 4500–7000 r.p.m. (turbines speed of rotation). As a consequence the manufacturer defined two operational speed ranges: 5350–5400 r.p.m. and 6100–6350 r.p.m. Hence the maximum operating speed was reduced to 6350 r.p.m. Twenty years later this limitation became unacceptable and since 1992 much work has been carried out in order to operate the turbine for the production of ultra viscous oil at a speed of 6800 r.p.m.

Tests and analyses have been performed by several teams including PETROBRAS-INSA [1, 2] and the University of Rio de Janeiro. This paper concerns the dynamic behaviour of this assembly and more specifically the dynamic behaviour when the speed

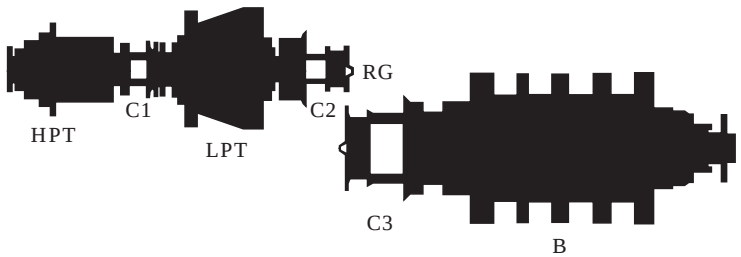

Figure 1. Schematic view of the turbine–blower assembly. HPT, High pressure turbine; LPT, low pressure turbine; B, Blower; C1, C2, C3, couplings; RG, reduction gear.

0022–460X/98/310047 + 16 $30.00/0

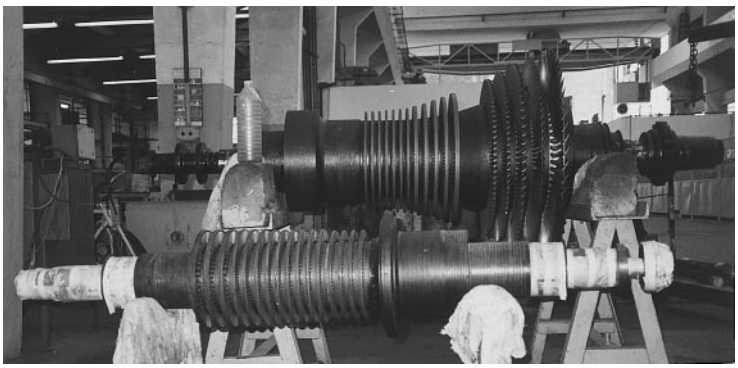

Figure 2. High Pressure Turbine (HPT) and Low Pressure Turbine (LPT) rotors.

of rotation of the two steam turbines is increased, by roughly ten per cent, from 6200 r.p.m. to 6800 r.p.m. The work presented in what follows deals with the dynamic behaviour of rotors and blades, and gives a practical engineering conclusion concerning this possible speed increase.

2. ROTORDYNAMICS

Following the collection of field data and from the geometry of the assembly it was necessary to determine the critical speeds of the turbine–blower machinery in torsion, to determine the critical speeds, the instability and the mass unbalance responses in bending where the three rotors are studied separately. Two spare rotors, respectively of the high pressure turbine (HPT) and of the low pressure turbine (LPT), are shown in Figure 2. Modelling and solving equations has been performed using the methods and computer codes shown in reference [3].

2.1. TURBINE–BLOWER ASSEMBLY IN TORSION

The ratio of the turbine speed of rotation N_T and the blower speed of rotation N_B is $N_T/N_B = 2{\cdot}55$. The finite element model is shown in Figure 3. The elements are shaft elements, disc elements and coupling elements including stiffness and mass characteristics. The set of equations to be solved can be written as:

$$\mathbf{M}\ddot{\boldsymbol{\delta}} + \mathbf{K}\boldsymbol{\delta} = \mathbf{0} \tag{1}$$

where $\mathbf{M}$ and $\mathbf{K}$ are respectively the mass and stiffness matrices and where $\boldsymbol{\delta}$ is the nodal displacement vector. The lowest frequencies and mode shapes are obtained by solving the

TABLE 1

Critical speeds in torsion

	Harmonic excitation							
Natural freq. (Hz)	$1N_B$	$2N_B$	$1N_T$	$3N_B$	$4N_B$	$5N_B$	$2N_T$	$3N_T$
F_1 (25·1)	3840	1920	1506	1280	960	768	753	502
F_2 (86·5)	–	6617	5190	4411	3308	2646	2595	1730
F_3 (91·5)	–	7000	5490	4666	3499	2799	2745	1830
F_4 (103·8)	–	7940	6228	5293	3970	3176	3114	2076

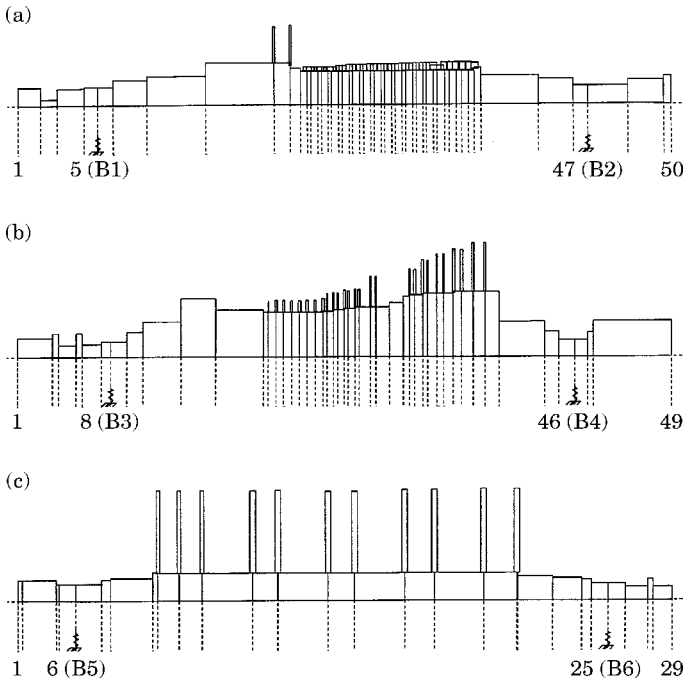

Figure 3. Finite element model of the turbine–blower assembly. (a) High pressure turbine, (b) low pressure turbine, (c) blower.

eigenvalue–eigenvector problem corresponding to (1). The Campbell diagram which shows the natural frequencies as a function of the speed of rotation and the possible critical speeds is presented in Figure 4 in which the four first frequencies, excluding the first frequency which is obviously zero, are presented. Critical speeds due to the turbine harmonics (N_T) and to the blower harmonics (N_B) are shown in Table 1.

$1N_B$, $2N_B$, $3N_B$, $4N_B$, $5N_B$ and $1N_T$, $2N_T$, $3N_T$ are respectively harmonics 1,2,3,4,5 of the blower and harmonics 1,2,3 of the turbine. It is clear that natural frequency $F_4 = 103{\cdot}8$ Hz gives a critical speed at 6228 r.p.m. due to harmonic $1N_T$ of the turbine, it is also clear

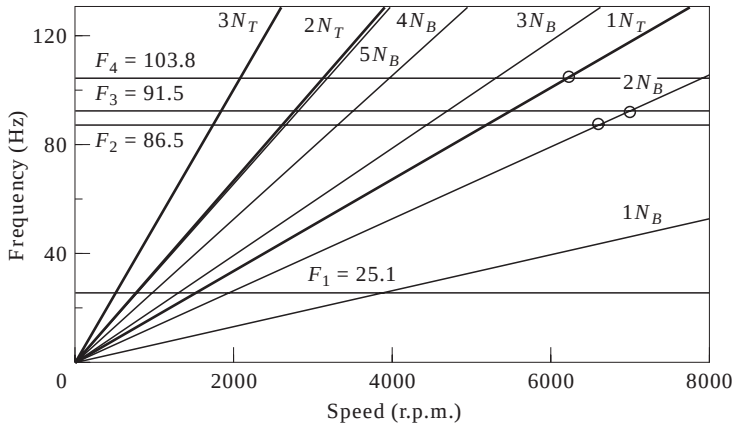

Figure 4. Campbell diagram for assembly in torsion: N_B, harmonic blower; N_T, harmonic turbines.

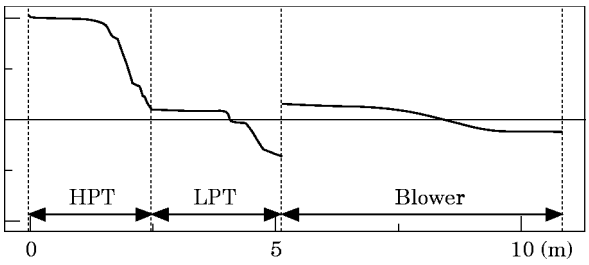

Figure 5. Mode shape of the mode $F_2 = 86{\cdot}5$ Hz.

that harmonic $2N_B$ of the blower gives two critical speeds: one at 6617 r.p.m. and one at 7000 r.p.m. corresponding respectively to $F_2 = 86{\cdot}5$ Hz and $F_3 = 91{\cdot}5$ Hz.

As the turbines have been operating for years at approximately 6200 r.p.m. the critical speed due to harmonic $1N_T$ does not cause any problem because of a low level of excitation and high associated damping. The critical speed 7000 r.p.m. is outside the future expected speed of rotation range. The critical speed of rotation 6617 r.p.m. due to F_2 and harmonic $2N_B$ is of great interest as it is situated in the future speed of rotation range and the corresponding mode shape is shown in Figure 5. It can be observed that the displacement amplitudes of the HPT are much higher than those of the LPT. This will be considered later when looking into blade dynamics.

2.2. TURBINES AND BLOWER IN BENDING

2.2.1. *Modelling*

Modelling the two turbines and the blower in bending [4] can be achieved separately. It includes shaft, disc and hydrodynamic bearing elements. Bearing modelling uses results from reference [5] and the set of equations to be solved can be written as:

$$\mathbf{M}\ddot{\boldsymbol{\delta}} + \mathbf{C}(\Omega)\dot{\boldsymbol{\delta}} + \mathbf{K}(\Omega)\boldsymbol{\delta} = \mathbf{F}(t), \tag{2}$$

where $\mathbf{M}$ is the symmetric mass matrix, $\mathbf{C}$ is the asymmetric matrix including an antisymmetric gyroscopic matrix function of the angular speed of rotation Ω and an asymmetric matrix owing to the characteristics of the bearings. The stiffness matrix includes characteristics of the bearings which are a function of Ω and shaft characteristics. Here $\mathbf{F}(t)$ is the mass unbalance force vector and $\boldsymbol{\delta}$ is the vector containing all the nodal displacements. The critical speeds, the Campbell diagram and possible instabilities stem from the solutions of

$$\mathbf{M}\ddot{\boldsymbol{\delta}} + \mathbf{C}(\Omega)\dot{\boldsymbol{\delta}} + \mathbf{K}(\Omega)\boldsymbol{\delta} = \mathbf{0} \tag{3}$$

sought in the form e^{rt}. Therefore, in general:

$$r_i = -\alpha_i\omega_i/\sqrt{1-\alpha_i^2} \pm j\omega_i, \tag{4}$$

where ω_i is the ith angular frequency, α_i is the ith modal damping ratio.

If $-\alpha_i\omega_i/\sqrt{1-\alpha_i^2}$ is a positive quantity the system is unstable. The mass unbalance response stems from the steady state solution of (2) with:

$$\mathbf{F}(t) = \mathbf{F}_1 \operatorname{Sin} \Omega t + \mathbf{F}_2 \operatorname{Cos} \Omega t. \tag{5}$$

TABLE 2

High pressure turbine

	Speed (r.p.m.)					
	6200			6800		
F_1 (Hz), α_1		60·66, 0·17			61·79, 0·16	
F_2 (Hz), α_2		92·56, 0·22			91·7, 0·20	
F_3 (Hz), α_3		105·3, 0·35			108·7, 0·32	
F_4 (Hz), α_4		160·6, 0·49			163·2, 0·45	
	(a_{max})	(ab_1)	(ab_2)	(a_{max})	(ab_1)	(ab_2)
Case 1 (μm)	29·8	19·9	21·8	25·4	17·4	17·8
Case 2 (μm)	21·0	16·3	15·0	26·7	20·3	19·1

As the machinery was more than 20 years old when this work was carried out, it was decided not to use the last American Petroleum Institute (API) standard [6] and to use the API standard published in 1979 for defining the mass unbalance *md*:

$$md = Mg/2\Omega^2 \approx 5M/\Omega^2, \tag{6}$$

where M is the rotor mass, $\boldsymbol{g}$ the gravity and where Ω is 105% of the maximum value of the speed of rotation. If the run-out is assumed to be zero, the same API standards recommend that the vibration level at the bearing locations should not exceed:

$$a = 1391/\sqrt{N}, \tag{7}$$

where N is the maximum continuous speed of rotation in r.p.m. and a is the single peak amplitude in micron. The procedure adopted here is a calculated simulation of the test recommended by API standards to discover the sensitivity of the rotors to unbalance when a critical speed is within the operating speed range.

Two cases are considered for the two turbines and the blower. In case 1, the mass unbalance *md* is located by the rotor's center of inertia, this case being related to the so-called cylindrical or translational mode. In case 2, the mass unbalance is divided into two equal quantities (md/2) which are in phase opposition and in general situated at the two ends of the rotor, this case being related to the so-called conical mode.

TABLE 3

Low pressure turbine

	Speed (r.p.m.)					
	6200			6800		
F_1 (Hz), α_1		41·42, 0·11			41·88, 0·11	
F_2 (Hz), α_2		69·14, 0·22			69·82, 0·21	
F_3 (Hz), α_3		106·6, 0·13			105·4, 0.12	
F_4 (Hz), α_4		186·5, 0·20			184·3, 0·18	
	(a_{max})	(ab_3)	(ab_4)	(a_{max})	(ab_3)	(ab_4)
Case 1 (μm)	35·8	25·0	23·0	38·8	26·0	24·7
Case 2 (μm)	30·5	20·8	14·3	29·0	19·3	13·5

TABLE 4

Blower

	Speed (r.p.m.)					
	2431			2667		
F_1 (Hz), α_1		–			–	
F_2 (Hz), α_2		–			–	
F_3 (Hz), α_3		24·95, 0·056			24·83, 0.052	
F_4 (Hz), α_4		27·12, 0·019			27·10, 0·014	
	(a_{max})	(ab_5)	(ab_6)	(a_{max})	(ab_5)	(ab_6)
Case 1 (μm)	101·0	5·3	5·8	89·8	0·9	2·4
Case 2 (μm)	44·8	37·0	26·5	59·5	48·1	37·7

2.2.2. *High pressure turbine*

The finite element model is shown in Figure 3. The mass unbalance responses at nodes 1, 5 (bearing 1), 47 (bearing 2) and 50 are respectively presented for case 1 and case 2 in Figures 6 and 7. Deflections at 6800 r.p.m. for cases 1 and 2 are shown in Figures 8 and 9. Natural frequencies, damping ratios and response amplitudes (maximum displacement and displacements at bearing 1 (ab_1) and at bearing 2 (ab_2) in cases 1 and 2) are presented in Table 2. Equation (7) gives a maximum displacement at bearing locations of 17·7 μm at 6200 r.p.m. and 16·9 μm at 6800 r.p.m. It is also clear that this rotor stays stable when the speed increases up to 6800 r.p.m.

2.2.3. *Low pressure turbine*

The finite element model is shown in Figure 3. The mass unbalance responses at nodes 1, 8 (bearing 3), 46 (bearing 4) and 49 are respectively presented for case 1 and case 2 in Figures 10 and 11. Deflections at 6800 r.p.m. for cases 1 and 2 are shown in Figures 12 and 13. Natural frequencies, damping ratios and response amplitudes (maximum displacement and displacements at bearing 3 (ab_3) and at bearing 4 (ab_4) in cases 1 and 2) are presented in Table 3. Equation (7) gives the same maximum displacement as for the high pressure turbine. It is also clear that this rotor stays stable when the speed of rotation increases up to 6800 r.p.m.

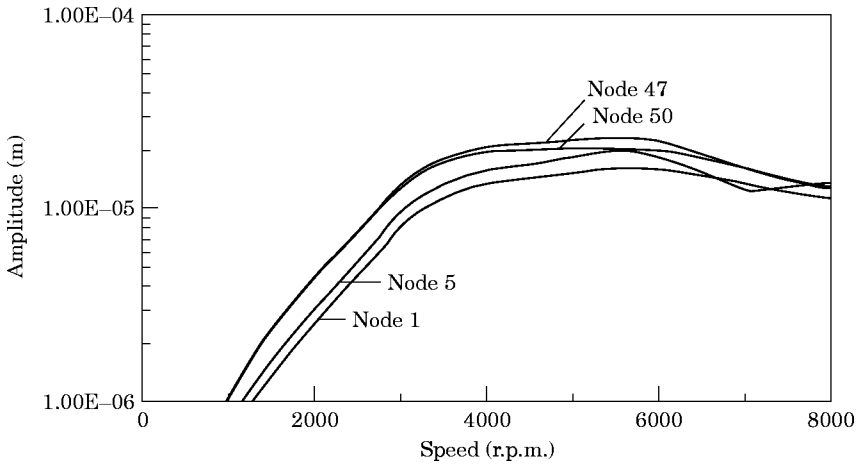

Figure 6. HPT response at nodes 1, 5, 47 and 50: case 1.

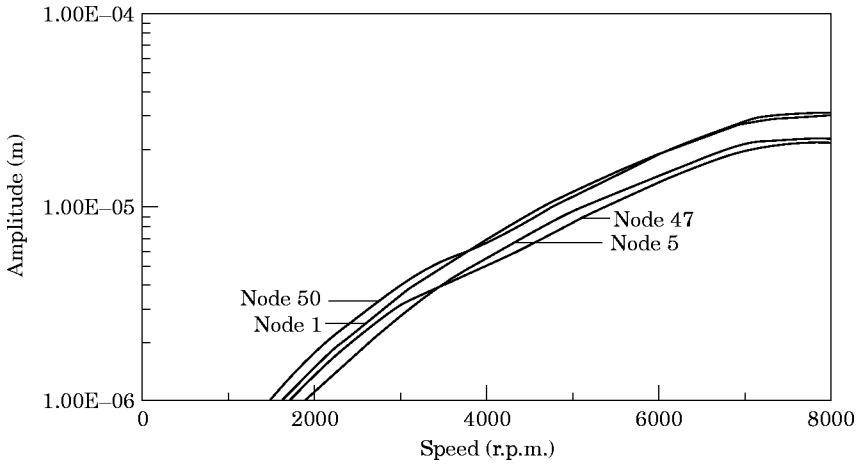

Figure 7. HPT response at nodes 1, 5, 47 and 50: case 2.

2.2.4. *Blower*

When the turbine rotors rotate at 6200 or 6800 r.p.m. the blower rotor rotates at 2431 or 2667 r.p.m. The finite element model is shown in Figure 3. The mass unbalance response at nodes 1, 6 (bearing 5), 25 (bearing 6) and 29 are respectively presented for case 1 and 2 in Figures 14 and 15. Deflections at 2667 r.p.m. for cases 1 and 2 are shown in Figures 16 and 17. Natural frequencies, damping ratios and response amplitudes (maximum displacement and displacements at bearing 5 (ab_5) and at bearing 6 (ab_6) in cases 1 and 2) are presented in Table 4.

Equation (7) gives a maximum displacement at bearing locations of 28 μm at 2431 r.p.m. and of 26·9 μm at 2667 r.p.m. This rotor stays stable when its speed of rotation increases up to 2667 r.p.m.

2.3. CONCLUSION ON ROTOR STUDIES

In torsion a critical turbine speed of 6617 r.p.m. could be problematic in that the result agrees with the experimental analyses which, fortunately, show significant torsional damping.

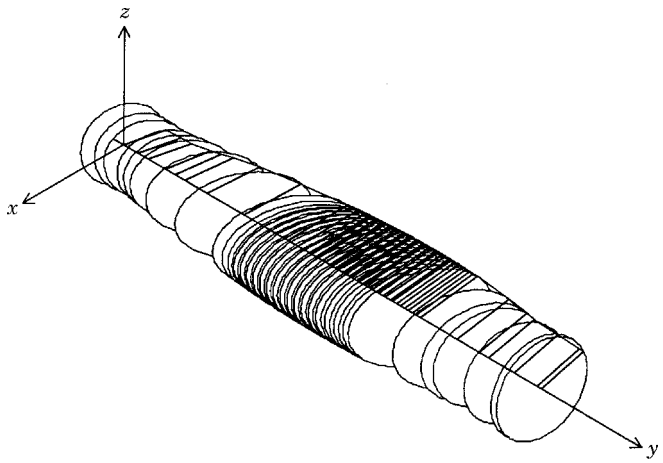

Figure 8. HPT deflection at 6800 r.p.m. for Case 1; maximum amplitude 25·4 μm.

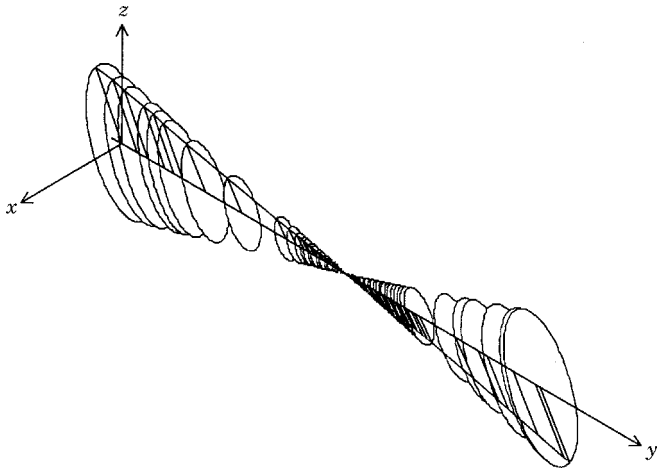

Figure 9. HPT deflection at 6800 r.p.m. for Case 2; maximum amplitude 26·7 μm.

In bending an increase of the speed of rotation does not significantly change the behaviour and the three rotors stay stable. The blower does not really satisfy all the API conditions on displacements, however, the machinery has been operating for 20 years without any problem.

3. BLADE DYNAMICS

The blower rotor contains five massive heavy impellers, and it was clear that increasing the speed of rotation of this rotor would not cause any problem to the impellers. Two kinds of problems related to turbine blades had to be solved. At first, it was necessary to know if the speed increase would give resonant conditions for the blades, then it was necessary to know the stresses due to the centrifugal effect and to the rotor vibration, excited at 6617 r.p.m. by the second torsional critical speed.

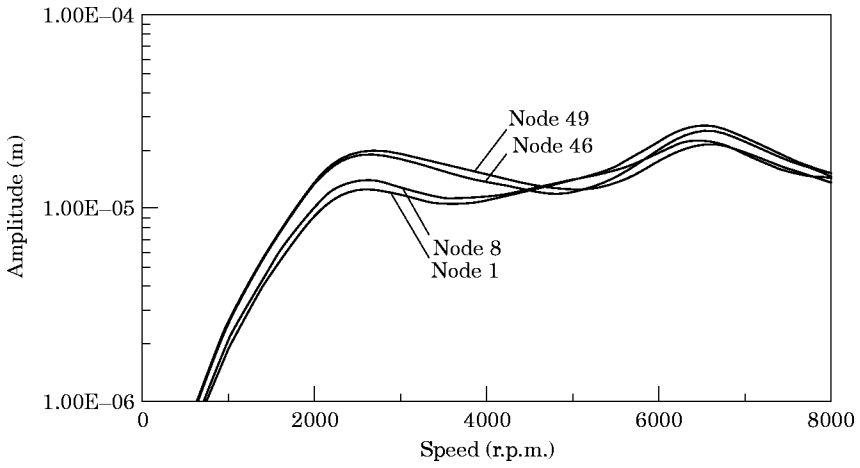

Figure 10. LPT response at nodes 1, 8, 46 and 49: case 1.

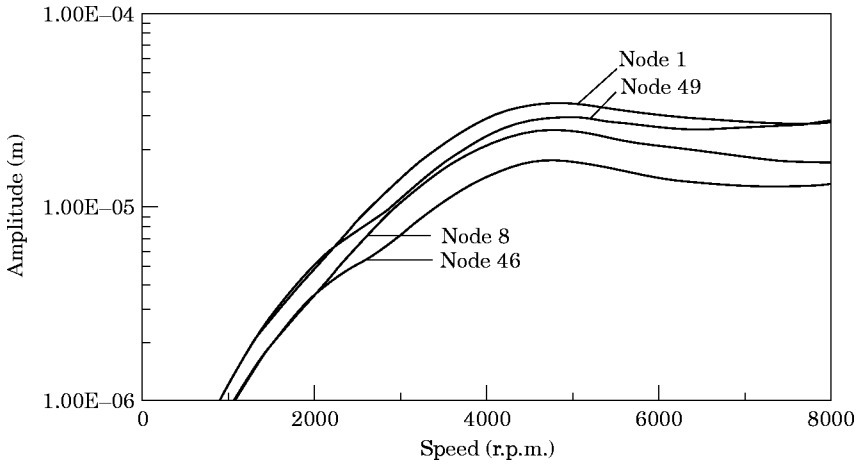

Figure 11. LPT response at nodes 1, 8, 46 and 49: case 2.

3.1. BLADE FREQUENCIES AND MODES

3.1.1. *Modelling*

The finite element model uses the three dimensional isoparametric element with 20 nodes and three degrees of freedom per node as it can be used for shrouded blades, as in Figure 18, and for wired twisted and untwisted blades, as in Figure 19.

The rotors ensure nearly ideal clamping conditions and all the blades can be assumed to be clamped at the root. Twenty five years after manufacturing this assembly, it was difficult to obtain all the data, in particular the material properties of the steel were assumed to be: Young's modulus $E = 2{\cdot}10^{11}$ N/m^2, density $\rho = 7800$ kg/m^3, Poisson's ratio $v = 0{\cdot}3$. Aerodynamic and structural damping were not considered, as they are quite low, and the gyroscopic effect, as the blades are radial, were not taken into account either. Blade modelling [7–9] gives a set of equations which can be written as:

$$\mathbf{M}\ddot{\boldsymbol{\delta}} + (\mathbf{K}_E + \mathbf{K}_G(\sigma_0) - \Omega^2\mathbf{M}_G)\boldsymbol{\delta} = \mathbf{F}_C(\Omega^2), \tag{8}$$

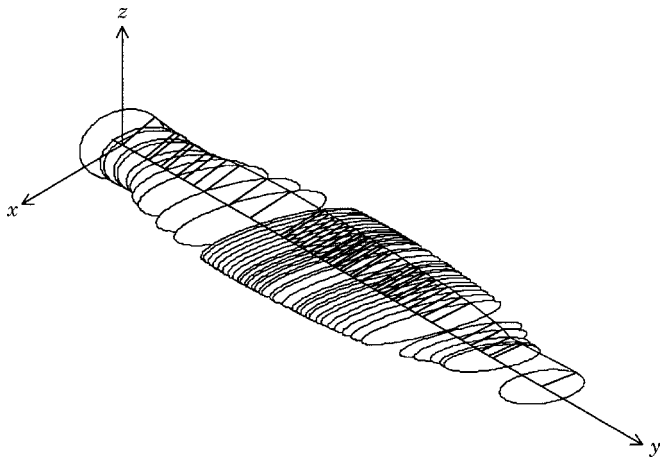

Figure 12. LPT deflection at 6800 r.p.m. for Case 1; maximum amplitude 38·8 μm.

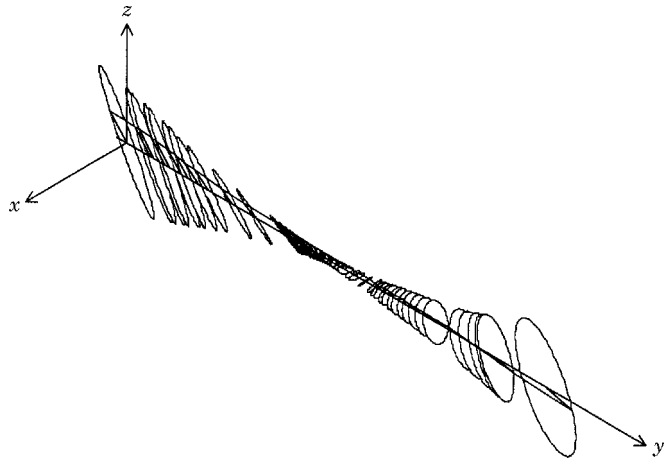

Figure 13. LPT deflection at 6800 r.p.m. for Case 2; maximum amplitude 29·0 μm.

where $\mathbf{M}$, $\mathbf{K}_E$, $\mathbf{K}_G(\sigma_0)$ and $\Omega^2\mathbf{M}_G$ are respectively the mass, the elastic stiffness, the geometric stiffness and the spin softening matrices. $\mathbf{F}_C(\Omega^2)$ and $\boldsymbol{\delta}$ are respectively the centrifugal force and the nodal displacement vectors. This set of non-linear equations can be partitioned into two sets. The first is:

$$(\mathbf{K}_E + \mathbf{K}_G(\sigma_0) - \Omega^2\mathbf{M}_G)\boldsymbol{\delta}_S = \mathbf{F}_C(\Omega^2), \tag{9}$$

which gives the static position $\boldsymbol{\delta}_S$ and the initial stresses σ_0 due to the rotation effect. The second set of equations is:

$$\mathbf{M}\ddot{\boldsymbol{\delta}}_d + (\mathbf{K}_E + \mathbf{K}_G(\sigma_0) - \Omega^2\mathbf{M}_G)\boldsymbol{\delta}_d = 0, \tag{10}$$

which gives the natural frequencies and the associated mode shapes around the static position obtained from equation (9). In the applications considered here, the blades are coupled by a shroud or by a wire and the entire assembly has to be considered. The size of this problem is made acceptable by taking into account the periodic characteristics of

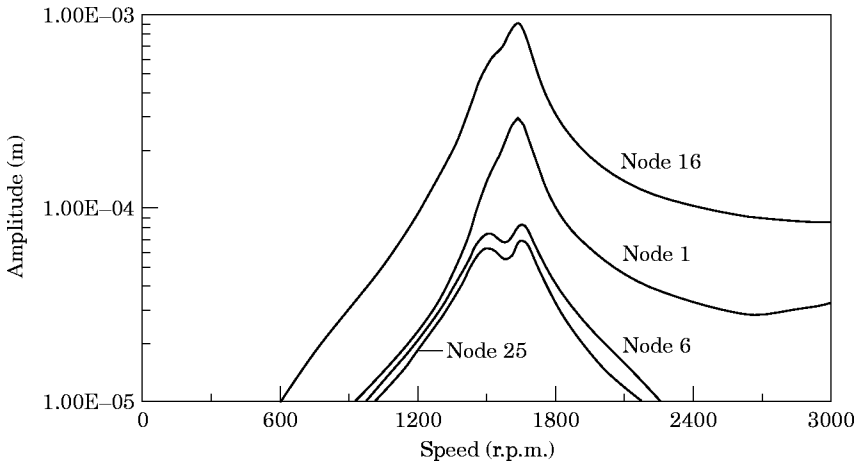

Figure 14. Blower response at nodes 1, 6, 16 and 25: case 1.

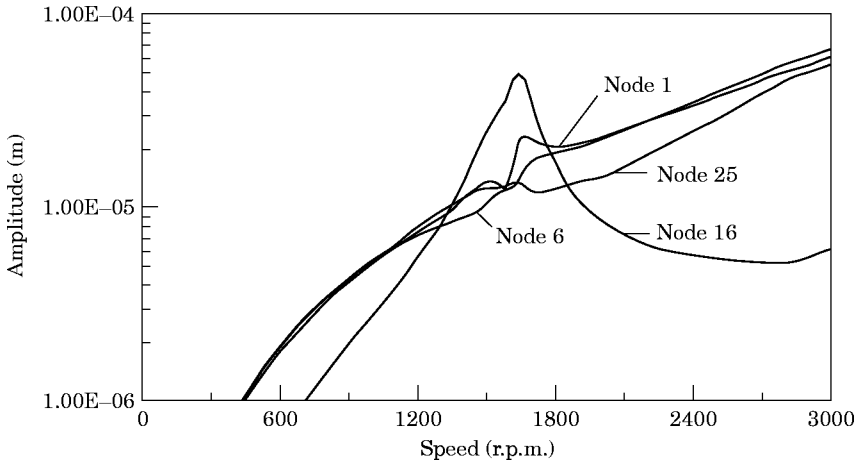

Figure 15. Blower response at nodes 1, 6, 16 and 25: case 2.

the system and a supplementary reduction based on a substructure method. For a blade alone there is a resonant condition for the ith frequency $f_i(\Omega^2)$ when:

$$f_i(\Omega^2) = nN_\Omega, \tag{11}$$

where n is the nth engine order (EO) and N_Ω the speed of rotation in revolutions per second.

For coupled blades, a resonant condition occurs when the frequency of the excitation equals one of the natural frequencies of the assembly and when the exciting force profile has the same shape as the associated natural mode of vibration. Consequently, resonance occurs when equation (11) is satisfied and when the number of nodal diameters ND equals the engine order EO simultaneously [10].

Many years of field experience on these turbines made it possible to decide to model 7 bladed assemblies: shrouded assembly 1, Figure 18, shrouded assembly 2 and wired assemblies 3, 4, 5, 6, 7, Figure 19. In what follows the presentation is limited to the high pressure turbine assembly 1 and to the highest low pressure turbine wired assembly 7.

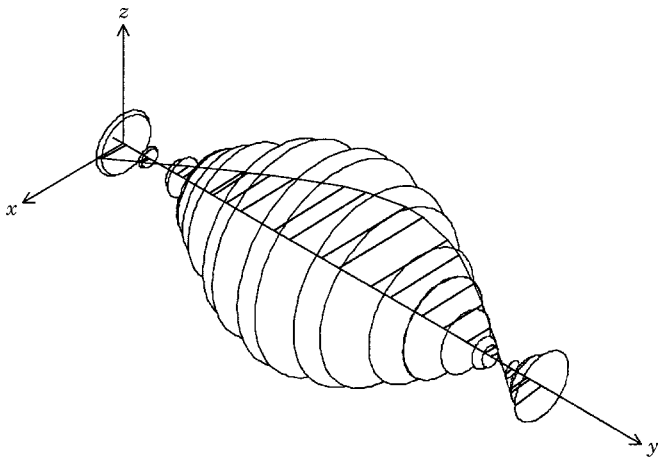

Figure 16. Blower deflection at 2667 r.p.m. for Case 1; maximum amplitude 89·8 μm.

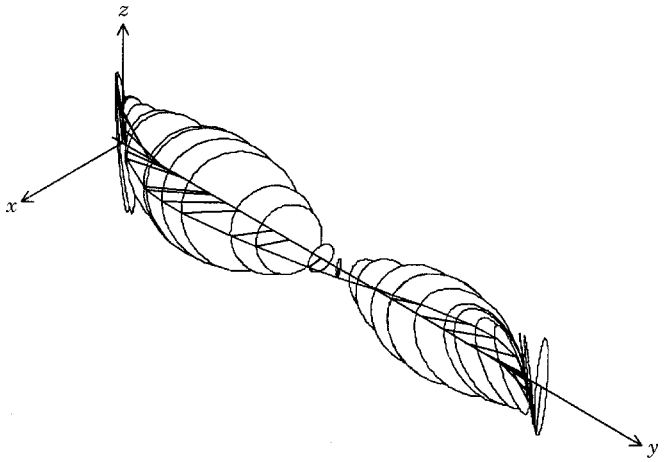

Figure 17. Blower deflection at 2667 r.p.m. for Case 2; maximum amplitude 59·5 μm.

3.1.2. *High pressure turbine shrouded assembly* 1

This stage consists of 44 shrouded untwisted blades, Figure 20. The shroud is continuous and 1/44 of the assembly is modelled, Figure 21. The frequencies calculated are very high and no excitation can be induced by an engine order lower than 14.

3.1.3. *Low pressure turbine wired assembly* 7

This stage consists of 57 wired and twisted blades. Here, specific difficulties in modelling come from the blade/wire contact effect. Only one blade and a portion of the wire is modelled. The finite element mesh, Figure 22, consists of about 200 finite elements and 1600 nodes. The design of the damping wires is mostly based on empirical data and experience and, due to their non-linear influence the dynamic behaviour of the assembly can only be estimated. Blade and wire are modelled independently and are linked by springs in the contact area: springs are assumed to be very stiff in the radial direction and less stiff in the circumferential direction, in order to permit relative wire/blade displacements. In the axial direction the wire follows the blades. The stiffness values were estimated using complementary three dimensional computations. Using this, the frequencies and the mode shapes of the entire turbine blading were computed for the 29 different possible number of modal diameters (ND from 0–28). When the number of nodal diameter increases, wire influence can be more significant. Some possible resonant

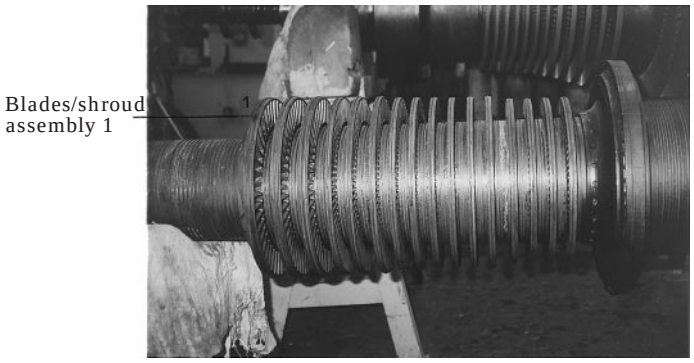

Figure 18. High pressure turbine rotor.

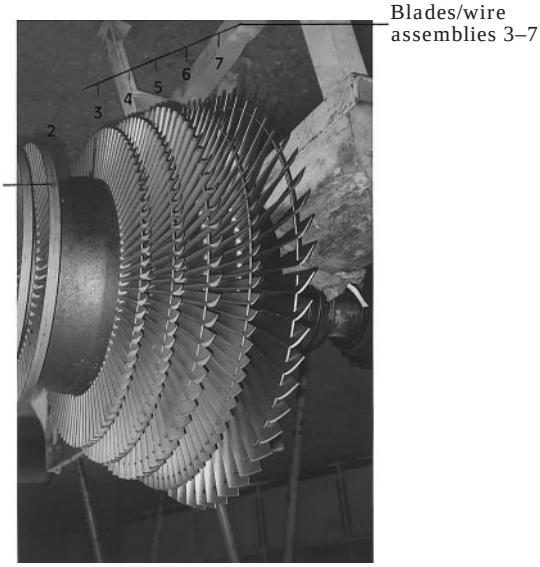

Figure 19. Low pressure turbine rotor.

conditions are shown in Figure 23 where the resonant condition in the operating range is for mode 2 and engine order 6.

3.2. DYNAMIC RESPONSE TO AN EXCITATION BY THE BASE

This problem concerns HPT blades and, more specifically, stage 1. The excitation is imposed by the torsional vibration of the rotor which gives a frequency twice the frequency of rotation of the blower and a critical speed of 6617 r.p.m. due to $2N_B$. The maximum

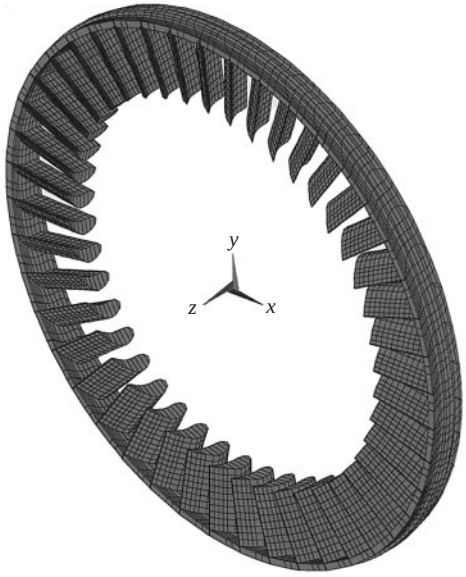

Figure 20. HPT shrouded assembly 1.

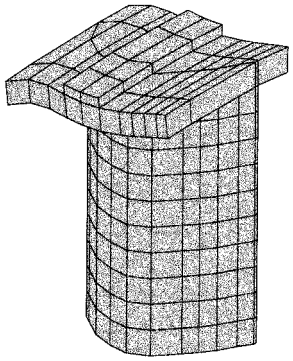

Figure 21. HPT shrouded assembly 1; cyclic symmetric sector (one blade and the associated shroud portion).

amplitude at the blade root was obtained from field tests: 0·13° and then 0·23 mm. A torsional motion of the rotor is only able to excite modes with 0 nodal diameter.

The response of the system was examined within the range from 6000–7000 r.p.m. At a rotation speed Ω, the frequency of excitation is:

$$fe = (\Omega/2{\cdot}55)*2/60 \text{ Hz}. \tag{12}$$

In a cylindrical co-ordinate system the displacement prescribed for each node of the root is:

$$\{\mathbf{d}\} = \begin{Bmatrix} 0 \\ 0{\cdot}2310^{-3} \\ 0 \end{Bmatrix} \cos(2\pi fe)t. \tag{13}$$

The displacements induced along the blade when the speed of rotation varies from 6000–7000 r.p.m. are constant: 0·3 mm at the blade tip and the Von Mises stresses are obtained from the 6 components of the stress in the XYZ co-ordinate system by:

$$\sigma_{VM} = \sqrt{[(\sigma_{XX} - \sigma_{YY})^2 + (\sigma_{YY} - \sigma_{ZZ})^2 + (\sigma_{ZZ} - \sigma_{XX})^2 + 6(\sigma_{YZ}^2 + \sigma_{ZX}^2 + \sigma_{XY}^2)]/2}. \tag{14}$$

The Von Mises stress map associated with the superposition of the centrifugal effect and the base excitation effect is presented in Figure 24 for $\Omega = 6617$ r.p.m. The stress at the root of the blade is about 50 Mpa. This value is much lower than the elastic limit of the material and is about 50% greater than the value induced by the centrifugal effects alone.

3.3. CONCLUSION ON BLADE STUDIES

No excitation can be generated by the lowest engine orders 1, 2, 3.

Figure 22. LPT wired assembly 7; cyclic symmetric sector (one blade and the associated wire portion).

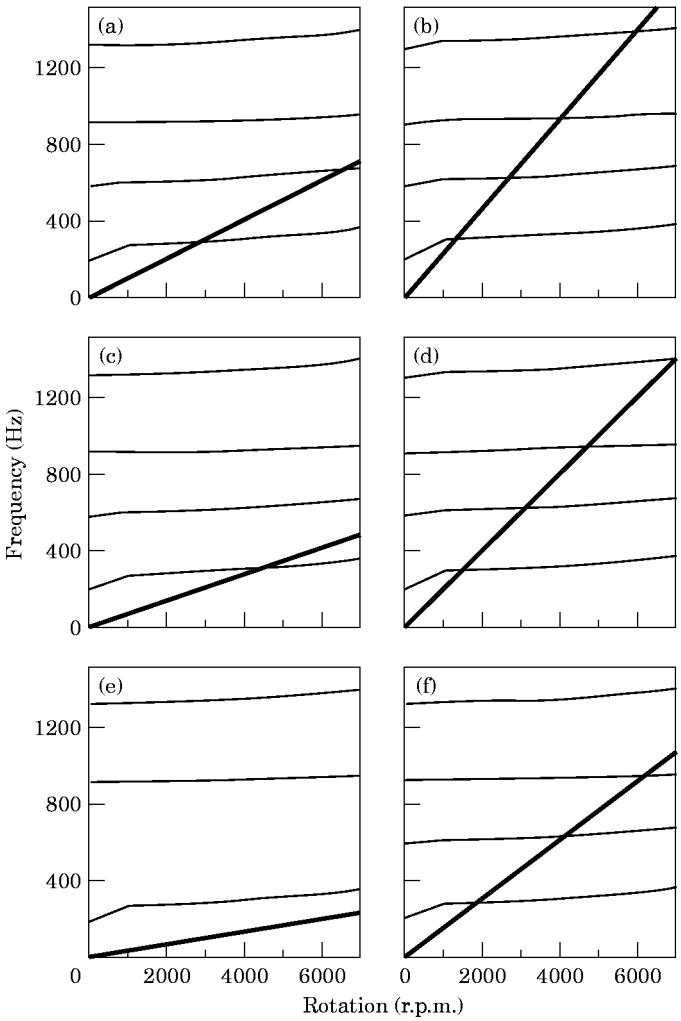

Figure 23. LPT wired assembly 7. Campbell diagrams for modes with 2, 4, 6, 9, 12 and 14 ND. (ND, number of nodal diameters; EO, engine order). (a) ND = EO = 6; (b) ND = EO = 14; (c) ND = EO = 4; (d) ND = EO = 12; (e) ND = EO = 2; (f) ND = EO = 9.

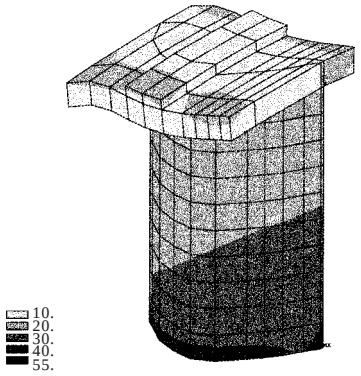

Figure 24. Excitation by the base for HPT shrouded assembly 1: Von Mises stress map.

Since the wire provides a fairly high level of damping, the other possible excitations should not be dangerous.

The Von Mises stresses, induced by the rotation and the torsional behaviour of the HPT rotor, are much lower than the fatigue strength of the material.

4. PRACTICAL ENGINEERING CONCLUSION

Following this study on the dynamic behaviour of a turbine/blower assembly, including both rotordynamic and blade dynamic aspects:

The turbine manufacturer agrees with a turbine speed increase up to 6800 r.p.m. as far as: (1) the components transmitting power, rotor and blades, are new; (2) certain blade profiles are modified. (3) The wired blades of the low pressure turbine are changed into shrouded blades. These modifications are presently being made on the rotors shown in Figure 2.

The reduction gear can be affected by certain slight modifications due to the speed increases. No change is required to the blower.

ACKNOWLEDGMENT

The authors would like to thank PETROBRAS for their financial support and for the permission to publish these results.

REFERENCES

1. A. Castilho, G. Gomes, G. Ferraris, K. Gjika and M. Lalanne 1997 7*th DINAME*, *Angra Dos Reis*, *Brazil*. Dynamic behavior of a turbine–blower assembly: behavior of rotors.
2. A. Castilho, G. Gomes, A. Berlioz, G. Jacquet-Richardet 1997 7*th DINAME*, *Angra Dos Reis*, *Brazil*. Dynamic behavior of a turbine–blower assembly: behavior of blades.
3. M. Lalanne and G. Ferraris 1997 *Rotordynamics Prediction in Engineering* Chichester: J. Wiley; second edition.
4. SYSROTOR© 1993 *Framasoft + CSI*, *Lyon*. Manuel de qualification.
5. P. E. Allaire *ROMAC* (*Rotating machinery and control research industrial program*.) *University of Virginia*.
6. American Petroleum Institute (API) 1995 *Mechanical Equipment Standards*.
7. D. J. Ewins and R. Henry 1988 *AGARD manual on Aeroelasticity in Axial Flow Turbomachines* **298**(2), Basic structural dynamics. Structural dynamic characteristics of individual blades, structural dynamic characteristics of bladed assemblies.
8. A. S. Panwalker, A. Rajamani and V. Ramamurti 1990 *The shock and Vibration Digest*, **22**(12), 3–9. Turbomachinery blade dynamics. A review.
9. G. Jacquet-Richardet, G. Ferraris and P. Rieutord 1996 *Journal of Sound and Vibration* **191**, 901–915. Frequencies and modes of rotating flexible blades disc–shaft assemblies: a global cyclic symmetry approach.
10. A. P. Singh and J. S. Vargo 1989 *ASME Journal of Engineering for Gas Turbine and Power* **111**, 601–609. Reliability evaluation of shrouded blading using the SAFE interference diagram.